J. Phys. Chem. Solids Vol. 49, No. 9, pp. 1035–1042, 1988
Printed in Great Britain.

0022-3697/88 $3.00 + 0.00


# A HIGHLY SENSITIVE METHOD FOR MEASUREMENT OF $^{222}$Rn PERMEABILITY IN METALS

S. K. PABI† and H. HAHN‡
FB 12.1, Bau 2, Werkstoffphysik, Univ. des Saarlandes, D-6600 Saarbrücken, West Germany

(*Received* 24 *August* 1987; *accepted in revised form* 30 *December* 1987)

**Abstract**—The spontaneous nuclear decay of a $^{226}$Ra needle provides an infinite source of $^{222}$Rn atoms, which permeate through the foil under investigation and result in a $^{222}$Rn-flux that can be measured on an atomic scale by counting the α-decay of $^{218}$Po, the first daughter product of $^{222}$Rn, collected on a surface barrier α-detector by application of an electrostatic field. The mathematical analysis of the measuring process provides the guidelines for the experiments as well as the basis for the quantitative estimation of the $^{222}$Rn flux. The role of different experimental variables and the method of standardization are reported. It is found that $^{222}$Rn dissolves in polycrystalline Au at low temperatures (e.g. 80°C) and its permeability varies with the thermal history of the specimen.

*Keywords:* Radon permeability, diffusivity, solubility in metals, permeation in Au, α-spectroscopy, mathematical model.

## 1. INTRODUCTION

The development of fusion reactor technology has, in recent years, drawn considerable attention to the permeation of gases in solids. The process is not well understood, and even for the same material the results may differ by many orders of magnitude [1]. In the case of diatomic gases the mechanism of dissociation of the gas molecules prior to their diffusion, and the presence/formation of surface layers on the specimens make the interpretation of the results all the more difficult. The permeability of $^{222}$Rn would be essentially free from these complications because Rn is a monoatomic gas which does not react with any metal [2]. The classical methods of measuring gas permeation rate are, however, unsuitable for $^{222}$Rn because of the extremely small flux involved. The present paper reports the development of an α-spectroscopic method along with its mathematical model for the estimation of $^{222}$Rn permeation flux on the atomic scale.

## 2. THE METHOD

Radioactive $^{226}$Ra undergoes a series of nuclear decays [3, 4] (Fig. 1) and it provides a practically infinite source of $^{222}$Rn gas (cf. Section 3.1). A $^{226}$Ra needle, fabricated as emanation standard of 56-μCi activity, was encapsulated in a 5-mm thick-walled brass container, as illustrated in Fig. 2. The open end of the capsule was sealed with an annealed 30-μm-thick Au-foil specimen (99.99% pure) and after about 5 weeks a nearly constant concentration of $^{222}$Rn was achieved in the sealed capsule (cf. Section 3.1). The temperature of the specimen was controlled to ±0.2°C and it could be varied rapidly (~15 K min$^{-1}$) by circulating oil around the brass capsule from two thermostats.

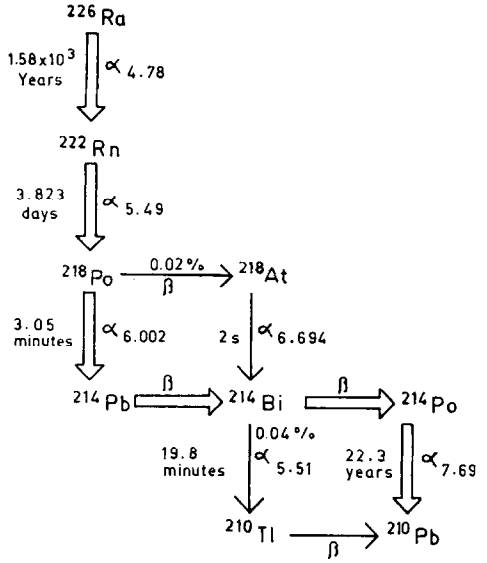


Fig. 1. The sequence of spontaneous nuclear decay of $^{226}$Ra along with the half-life of each component [3, 4]. The hollow arrows indicate the main reaction path and the thin arrows illustrate the secondary route taken up by a small percentage (indicated) of atoms. α and β refer to the type of decay and the subscript of α represents the maximum energy of this decay in MeV.

† Present address: Department of Metallurgical Engineering, Indian Institute of Technology, Kharagpur 721302, India.

‡ Present address: Materials Science Department, University of Illinois, Urbana, IL 61801, U.S.A.

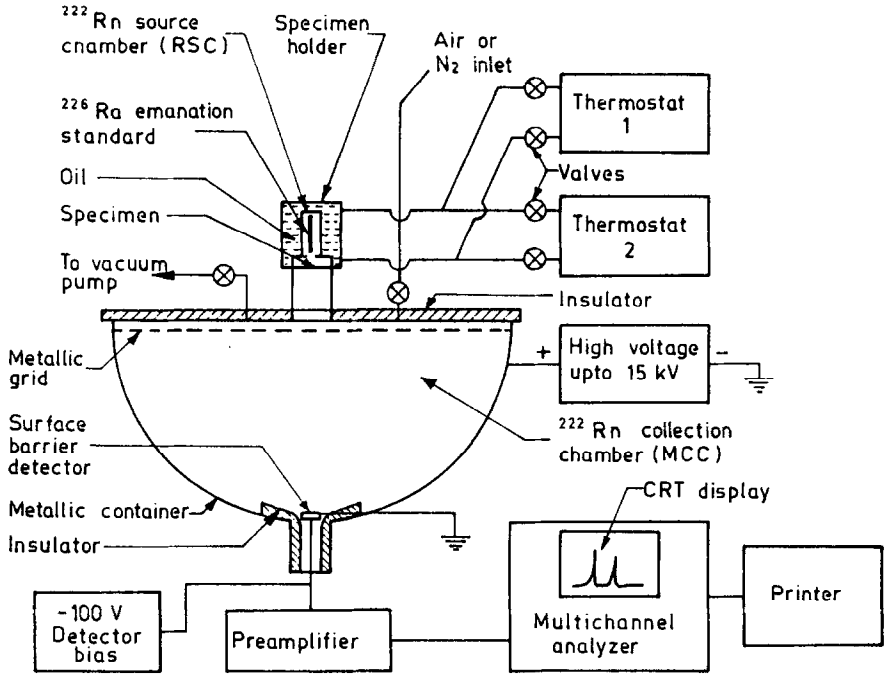


Fig. 2. Schematic illustration of the $^{222}$Rn diffusion measuring method.

When the sample holder was coupled with the detector assembly (Fig. 2), $^{222}$Rn diffusing from the source chamber (RSC) through the foil specimen accumulated in a hemispherical metallic collection chamber (MCC) fitted with a metallic grid at the top and an ORTEC surface barrier $\alpha$-detector at the bottom. Normally, the active area of the $\alpha$-detector was 150 mm$^2$. The MCC along with the grid was maintained at a high positive voltage (e.g. 8 kV) and the $\alpha$-detector surface was held at ground potential. The ions of $^{218}$Po produced by the nuclear decay of $^{222}$Rn (cf. Fig. 1) within the MCC were deposited onto the surface of the $\alpha$-detector under the influence of the imposed electric field. The number of $\alpha$-decays of the $^{218}$Po atoms on the detector surface was recorded by a Nuclear Data multichannel analyzer fitted with an ORTEC preamplifier and EPSON printer (Fig. 2). The flux of $^{222}$Rn through the metal foil is calculated from the rate of the $\alpha$-decays of $^{218}$Po (cf. Section 3). The high efficiency of the electrostatic collection [5] of $^{218}$Po coupled with the absence of background in the $\alpha$-spectroscopy make the detection of $^{222}$Rn flux on atomic scale (e.g. $10^4$ atom m$^{-2}$s$^{-1}$) feasible by the present technique.

## 3. MATHEMATICAL MODEL

The measuring method is conceptually subdivided into four stages connected in series as follows:

(1) the building-up of $^{222}$Rn concentration in the RSC,

(2) its diffusion through the specimen,

(3) the accumulation of $^{222}$Rn in the MCC and formation of $^{218}$Po by its natural decay,

(4) the deposition of $^{218}$Po on the surface of the $\alpha$-detector and its decay.

### 3.1. *Analysis of Stage* 1

The variation of the number of $^{222}$Rn atoms $M_{Rn}$ in RSC produced by the $^{226}$Ra needle depends on the activity of the emanation standard $A_{Ra}$, the decay constant $\lambda_{Rn}$ of $^{222}$Rn and its flux $vM_{Rn}$ through the foil specimen, where $v$ is a constant for steady-state flow, i.e.

$$M_{Rn} = \frac{A_{Ra}}{(\lambda_{Rn} + v)} \{1 - \exp[-(\lambda_{Rn} + v)\theta]\}, \quad (1)$$

$\theta$ being the time (in s) elapsed after sealing the RSC with the foil specimen. $v$ is usually negligible at room temperature. Equation (1) shows that $M_{Rn}$ reaches 99.8% of its maximum limit $M_{Rn(\infty)}$ at $\theta \simeq 3 \times 10^6$ s (i.e. $\approx 5$ weeks). It is also apparent that for $A = 56\,\mu$Ci an outflow of $1.5 \times 10^5$ Rn atom s$^{-1}$ through the specimen can diminish $M_{Rn(\infty)}$ up to $\sim 7\%$. Since the flow rate of Rn is usually much smaller, the $^{226}$Ra needle provides a nearly constant number of $^{222}$Rn atoms in the (sealed) RSC during permeability measurements.

### 3.2. *Model for Stage* 2

Suppose (i) the solubility of $^{222}$Rn in the specimen depends only on its partial pressure and the temperature, (ii) the $^{222}$Rn transfer process across the gas–metal interfaces is much faster than its diffusion

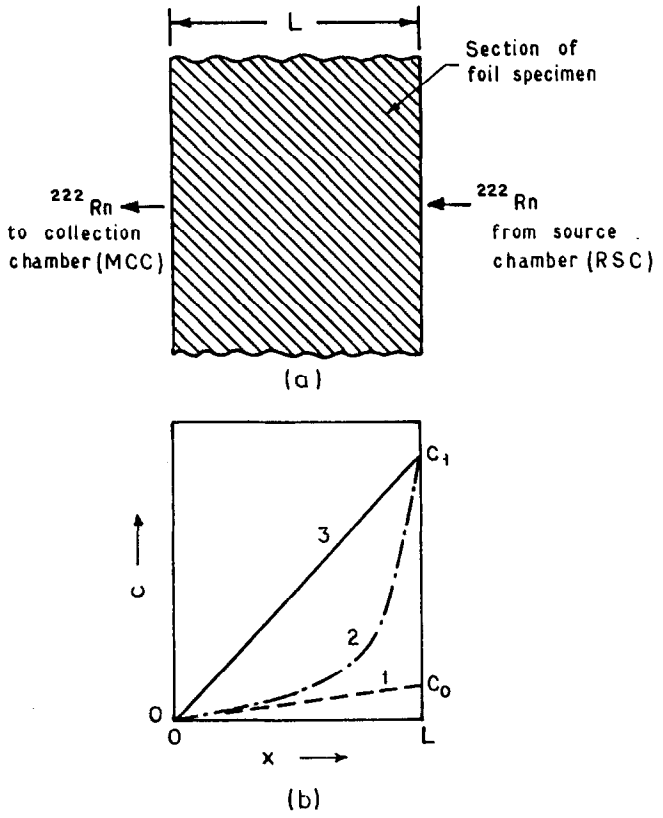


Fig. 3. (b) Schematic view of the variation of $^{222}$Rn concentration across the foil section displayed in (a). Curves 1 and 3 represent the steady-state concentration profiles at $T_0$ and $T_1$, respectively. Curve 2 corresponds to a non-steady state following up-quenching from $T_0$ to $T_1$.

through the foil, (iii) the gas volume† in RSC ($v_1 \approx 0.3$ ml) is much smaller than that in MCC ($v_2 = 5.87$ or 0.142 l) and (iv) the nuclear decay of $^{222}$Rn in the foil is negligible. The time-modulation of the $^{222}$Rn concentration profile (cf. Fig. 3) following pulse heating from $T_0$ to $T_1$ at time $t = 0$ takes place under the boundary conditions

$$C = C_0 \frac{x}{L}, \quad 0 \leqslant x \leqslant L, \quad t = 0, \tag{2}$$

$$C = 0, \qquad x = 0, \quad t \geqslant 0, \tag{3}$$

$$C = C_1, \qquad x = L, \quad t > 0, \tag{4}$$

where concentrations $C$, $C_0$ and $C_1$ are expressed in terms of the number of $^{222}$Rn atoms $\mu m^{-3}$. The field equation for diffusion of a non-decaying gas through the foil is

$$\frac{\partial C}{\partial t} = D \frac{\partial^2 C}{\partial x^2}, \quad 0 \leqslant x \leqslant L, \tag{5}$$

where $D$ is the $^{222}$Rn diffusivity at $T_1$, presumably independent of $C$. If $A$ is the area of the foil available for permeation,‡ it may be readily shown [6] that the total number of (nondecaying) $^{222}$Rn atoms accumulated in MCC at time $t$ is

$$n_t = \frac{ADC_1}{L}\left\{t - \frac{2L^2}{\pi^2 D}\sum_{n=1}^{\infty}\frac{(-1)^n}{n^2} \times\left[\exp\left(-\frac{n^2\pi^2 Dt}{L^2}\right)-1\right] - \frac{2C_0L^2}{C_1\pi^2 D} \times \sum_{m=0}^{\infty}\frac{1}{(2m+1)^2}\left[\exp\left(-\frac{(2m+1)^2\pi^2 Dt}{L^2}\right)-1\right] + \frac{C_0L^2}{2C_1\pi^2 D}\sum_{m=1}^{\infty}\frac{1}{m^2} \times\left[\exp\left(-\frac{4m^2\pi^2 Dt}{L^2}\right)-1\right]\right\}. \tag{6}$$

† In actual design a considerable portion of RSC is occupied by the $^{226}$Ra needle and its jacket.

‡ If the permeation takes place exclusively by a grain-boundary mechanism at low temperatures, $A \simeq f_{GS} \cdot \delta_1$, where $f_{GS}$ is the total length of grain boundary in the exposed foil area and $\delta_1$ is the effective grain-boundary thickness. The $^{222}$Rn transfer from grain boundary to the grain interior is assumed to be negligible and, naturally, $D$ as well as $C$ would then correspond to the grain-boundary region.

The decay of $^{222}$Rn in the foil can be taken into account by applying Danckwert's method [6] to the modified field equation

$$\frac{\partial C}{\partial t} = D\frac{\partial^2 C}{\partial x^2} - \lambda_{Rn} C.$$

Under such conditions,

$$n_t = \frac{ADC_1}{L}\left\{t + 2\sum_{n=1}^{\infty}(-1)^n \times \left[\frac{\lambda_{Rn}}{\delta}t + (1-e^{-\delta t})\left(\frac{\sigma-\lambda_{Rn}}{\delta^2}\right)\right] + \frac{2C_0}{C_1} \times \sum_{m=0}^{\infty}\left[\frac{\lambda_{Rn}}{\beta}t + (1-e^{-\beta t})\left(\frac{\beta-\lambda_{Rn}}{\beta^2}\right)\right] - \frac{2C_0}{C_1} \times \sum_{m=1}^{\infty}\left[\frac{\lambda_{Rn}}{\gamma} - (1-e^{-\gamma t})\left(\frac{\gamma-\lambda_{Rn}}{\gamma^2}\right)\right]\right\}, \quad (7)$$

where

$$\delta = (n^2\pi^2 D + \lambda_{Rn}L^2)/L^2 \quad (8)$$

$$\beta = [(2m+1)^2\pi^2 D + \lambda_{Rn}L^2]/L^2 \quad (9)$$

and

$$\gamma = (4m^2\pi^2 D + \lambda_{Rn}L^2)/L^2. \quad (10)$$

The foil thickness can be controlled in such a way that $\pi^2 D \gg \lambda_{Rn}L^2$, and then $\delta \simeq n^2\pi^2 D/L^2$, $\beta \simeq (2m+1)^2\pi^2 D/L^2$, and $\gamma \simeq 4m^2\pi^2 D/L^2$. Consequently, eqn (7) yields the value of $n_t$ at sufficiently large $t$, i.e.

$$n_{ts} = \left[\frac{ADC_1}{L} - \frac{AL\lambda_{Rn}}{6}(C_1 - C_0)\right]t - \frac{AC_1L}{6}\left(1 - \frac{C_0}{C_1}\right). \quad (11)$$

If $D \gtrsim 5 \times 10^{-15}$ m$^2$ s$^{-1}$, $L\lambda_{Rn}(C_1 - C_0)/6$ can be made negligible compared with $DC_1/L$ by suitably selecting the foil thickness $L$. And in that case, eqn (11) simplifies to

$$n_{ts} = \frac{ADC_1}{L}\left[t - \frac{L^2}{6D}\left(1 - \frac{C_0}{C_1}\right)\right]. \quad (12)$$

Physically this means that, if $6D \gg \lambda_{Rn}L^2$, the loss of $^{222}$Rn atoms in the foil becomes negligible, which would be taken for granted in the ensuing analysis. Following Barrer's definition [7], eqn (12) shows that the time-lag in establishing a steady-state $^{222}$Rn flow through the foil after a sudden rise of temperature from $T_0$ to $T_1$ is

$$S_2 = \frac{L_2}{6D}\left(1 - \frac{C_0}{C_1}\right). \quad (13)$$

### 3.3. *Computations for Stage 3*

For the time being it is assumed that the time-lag in Stage 3, i.e. $S_3$, is nil. The number of $^{222}$Rn atoms $N_t$ present in MCC at time $t$ is related to the incoming flux $dn_t/dt$ as follows:

$$\frac{dN_t}{dt} = \frac{dn_t}{dt} - kN_t, \quad (14)$$

where $k$ is an effective decay constant of $^{222}$Rn, which includes adsorption on and solution in the MCC walls and leakage from a particular detector assembly as well as the radioactive decay. Substituting (6) in (14) and integrating with respect to $t$ along with the initial condition $N_t = 0$ at $t = 0$ yields

$$N_t = \frac{ADC_1 e^{-kt}}{L}\left\{\int_0^t e^{kt}\,dt + 2\sum_{n=1}^{\infty}(-1)^n \times \int_0^t \exp\left[\left(k - \frac{n^2\pi^2 D}{L^2}\right)t\right]dt + \frac{2C_0}{C_1} \times \sum_{m=0}^{\infty}\int_0^t \exp\left[\left(k - \frac{(2m+1)^2\pi^2 D}{L^2}\right)t\right]dt - \frac{2C_0}{C_1}\sum_{m=1}^{\infty}\int_0^t \exp\left[\left(k - \frac{4m^2\pi^2 D}{L^2}\right)t\right]dt\right\}. \quad (15)$$

### 3.4. *Characteristics of the detector assembly*

Imagine a steady-state $^{222}$Rn flux of $\bar{N}_{Rn}$ atoms s$^{-1}$ entering MCC at $t = 0$. The number of $^{222}$Rn atoms in MCC is then given by

$$\bar{N}_t = \frac{\bar{N}_{Rn}}{k}(1 - e^{-kt}). \quad (16)$$

If $N_{Po}$ is the number of $^{218}$Po atoms collected by the silicon detector surface, and $\lambda_{Po}$ is the natural decay constant of $^{218}$Po,

$$\frac{dN_{Po}}{dt} = h\lambda_{Rn}\bar{N}_t - \lambda_{Po}N_{Po}, \quad (17)$$

where the collection factor $h$ is the fraction of $^{218}$Po atoms in MCC deposited on the detector. Integration with respect to $t$ subject to the initial condition $N_{Po} = 0$ at $t = 0$ gives

$$N_{Po} = \frac{h\lambda_{Rn}\bar{N}_{Rn}}{k\lambda_{Po}(\lambda_{Po} - k)} \times [\lambda_{Po}(1 - e^{-kt}) - k(1 - e^{-\lambda_{Po}t})]. \quad (18)$$

Since $\lambda_{Po} = 3.79 \times 10^{-3}$ s$^{-1}$ and $k$ is of the order of $10^{-6}$ s$^{-1}$ (cf. Section 4.1), $\lambda_{Po} - k \simeq \lambda_{Po}$. For small values of $kt$, eqn (18) may be simplified as

$$N_{Po} = \frac{h\lambda_{Rn}\bar{N}_{Rn}}{\lambda_{Po}}\left(t - \frac{1}{\lambda_{Po}}\right), \quad t > 1200\text{ s}, \quad kt \ll 1. \quad (19)$$

Therefore, the time-lag at the detector assembly in registering a steady-state flux is

$$S_4 = 1/\lambda_{Po}. \quad (20)$$

$\bar{N}_{Rn}$ can be estimated from the counting rate $I$ of the $\alpha$-decay from $^{218}Po$ according to the relation

$$\bar{N}_{Rn} = \left(\frac{dI}{dt}\right) \Big/ uhG\lambda_{Rn}, \quad t > 1200\,s, \quad kt \ll 1, \quad (21)$$

where the geometric efficiency of the detector $G$ is equal to 0.5 for $4\pi$-emission, and $u$ is the fraction of $^{218}Po$ atoms which undergoes $\alpha$-decay. The net collection efficiency $f(=uh)$ is evaluated from experiments (cf. Section 4.1).

### 3.5. *Mathematical model for Stage 4 coupled with Stages 2 and 3*

If the time-lag $S_3$ in Stage 3 is ignored (cf. Section 3.3) conceptually Stages 2 and 4 become directly connected in succession for time-lag calculation. Since $N_{Po} = 0$ at $t = 0$,

$$N_{Po} = e^{-\lambda_{Po}t} \int_0^t N_t e^{\lambda_{Po}t}\, dt, \quad (22)$$

where $N_t$ is given by eqn (15). If $L$ is selected in such a way that $kL^2 \ll \pi^2 D$, the integral in eqn (22) can be evaluated. Further simplification is possible by noting that $\lambda_{Po}^2$, $\lambda_{Po}k$ and $k^2$ are $\ll 1$ and negligible, since $\lambda_{Po} \gg k$, $\lambda_{Po} - k \simeq \lambda_{Po}$. If $kt \ll 1$, $(1 - e^{-kt}) \simeq kt$ and then the solution of eqn (22) gives the number of $^{218}Po$ atoms depositing on the detector surface. The steady-state $^{218}Po$ decay counting rate $I_s$ at sufficiently large $t$ is computed in a manner similar to that in Section 3.4. Thus,

$$I_s = \frac{fGADC_1\lambda_{Rn}}{L} \times \left[t - \left(\frac{1}{\lambda_{Po}} + \frac{L^2}{6D} - \frac{L^2}{6D}\frac{C_0}{C_1}\right)\right], \quad kt \ll 1. \quad (23)$$

Equation (23) shows that the time-lag $S_{24}$ in this case is equal to

$$\left(\frac{1}{\lambda_{Po}} + \frac{L^2}{6D} - \frac{L^2}{6D}\frac{C_0}{C_1}\right).$$

Comparison with eqns (13) and (20) indicates that $S_{24} = S_2 + S_4$, i.e. when Stages 2 and 4 are connected in series, the net time-lag of the combined system is equal to the sum of the time-lags of the constituent stages. By extending this argument to the entire measuring process, the net time-lag for a pulse-heating experiment may be written as

$$S = S_T + S_2 + S_3 + S_4, \quad (24)$$

where $S_T$ is the finite time taken by the specimen temperature to rise from $T_0$ to $T_1$. The magnitudes of $S_T$ and $S_3$ can be determined experimentally. Equation (24) ignores the effect of Stage 1, because the diffusion measurements start after attaining steady-state in Stage 1 (cf. Sections 2 and 3.1).

The steady-state $^{222}Rn$ flux through the foil $N_{Rn}$ can be estimated from eqn (23) which, in turn, gives $DC_1$. It follows that

$$N_{Rn} = \frac{DC_1}{L} = \frac{\left(\frac{dI_s}{dt}\right)}{fGA\lambda_{Rn}}, \quad kt \ll 1. \quad (25)$$

For an ideal specimen in which permeation takes place either through the grain boundaries (which is more probable) or through the grains, it is now possible to evaluate $D$, $C_0$ and $C_1$ from the measure of time-lags and $N_{Rn}$ for various combinations of $T_0$ and $T_1$ in pulse-heating experiments.

## 4. RESULTS AND DISCUSSION

### 4.1. *Standardization of the measuring technique*

Figure 4 displays a typical spectrum of $\alpha$-decay recorded after introducing some $^{222}Rn$ atoms in MCC and it shows that the background is almost zero. The absence of the $\alpha$-decay peak from $^{222}Rn$ and 5.49 MeV (cf. Fig. 4) indicates that these atoms are not influenced by the applied electrostatic field.

Two detector assemblies, namely, MCC1 with $v_2 = 5.871$ and MCC 2 with $v_2 = 0.1421$ were used in the measurements. For the determination of the net collection efficiency $f$, air was allowed to pass gently through a standard $^{226}Rn$ solution of 100 pCi activity and fill the pre-evacuated MCC1, thereby obtaining a known number of $^{222}Rn$ atoms in MCC1. The rate of $^{218}Po$ decay recorded thereafter yields $f$. The MCC2, because of its small volume, was calibrated

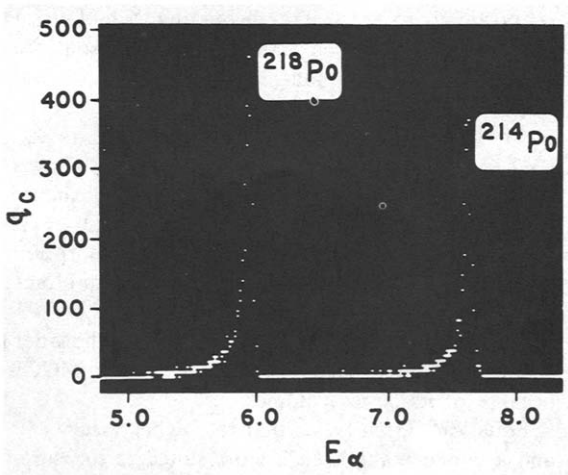


Fig. 4. A typical $\alpha$-decay spectrum recorded. Here $q_c$ is the cumulative number of counts per channel per cycle of 1000 s, and $E_\alpha$ is the energy of $\alpha$-emission in MeV.

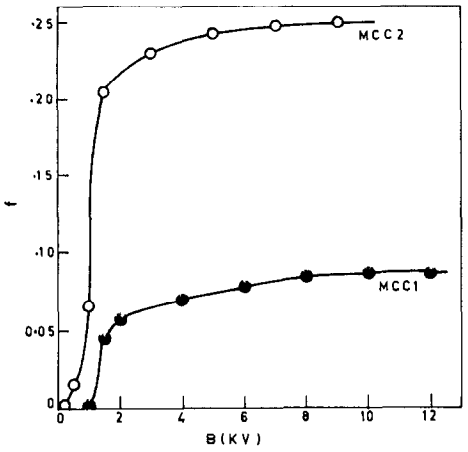


Fig. 5. Variation of the net collection efficiency $f$ with the applied positive bias of the MCC walls.

with respect to MCC1. The variation of $f$ with the applied positive bias $B$ of the MCC wall (cf. Fig. 5) reveals the existence of a threshold voltage $B_m$ below which $f \approx 0$. The $B_m$ increases with $v_2$. When $B > B_m$, $f$ increases initially rapidly with $B$ and approaches a saturation limit (cf. Fig. 5) which for MCC2 is about three times higher than that for MCC1. In all subsequent measurements $B$ was maintained at 8 kV for MCC1 and at 4 kV for MCC2. The $f$ value for MCC1 could almost be doubled by using an $\alpha$-detector with an active area of 300 mm$^2$ instead of 150 mm$^2$.

The effective decay constant $k$ was determined from the rate of loss of a fixed amount of $^{222}$Rn from MCC1 and MCC2. The gas inlets were sealed by dummy specimen holders and the number of $\alpha$-decays from $^{218}$Po counted in intervals of 1000s; $W_I$ was recorded with respect to time $t$. It was found that ln $W_I$ was linearly related to $t$, which confirms that the rate of loss of $^{222}$Rn by leakage from MCC and by adsorption or solution at the MCC walls is proportional to the instantaneous number of $^{222}$Rn atoms in MCC. The $k$ value determined from the slope of ln $W_I$ vs $t$ plots, was $2.59 \times 10^{-6}$ s$^{-1}$ for MCC 1 and $11.156 \times 10^{-6}$ s$^{-1}$ for MCC2. For a good detector assembly $k$ should be close to $\lambda_{Rn}$ ($=2.1 \times 10^{-6}$ s$^{-1}$). The surface area in MCC1 was $\sim$12.5 times larger than that in MCC2; and hence the larger values of $k$ for MCC2 indicate that, apart from nuclear decay, leakage rather than adsorption or solution is responsible for the loss of $^{222}$Rn atoms from MCC. The airtight seals of MCC2 and MCC1 were identical. The lower leakage rate from the latter is due to the lower partial pressure of $^{222}$Rn in MCC1 because of its larger volume.

Equation (23) suggests that the higher values of $f$ and $k$ would make MCC2 more suited to measurements of very small permeation flux (e.g. $10^4$ atoms m$^{-2}$ s$^{-1}$) over a short duration ($t < 80{,}000$ s), while MCC1 is preferable for measuring relatively stronger flux ($\geqslant 4 \times 10^4$ atoms m$^{-2}$ s$^{-1}$) over a longer period ($t < 80{,}000$ s). For permeability measurements over a prolonged period, $^{222}$Rn accumulated in MCC was flushed away from time to time by injecting high-purity $N_2$ gas, which makes $(1 - e^{-kt}) \simeq kt$ (cf. Section 3.5).

### 4.2. *Measurements on* Au *at low temperatures*

The specimen holder was held at 25°C for 5 weeks after sealing the RSC with Au foil. No $^{222}$Rn flux could be detected even after the specimen was heated up to 80°C within 7000 s. The subsequent heat-treatment schedule is displayed in Fig. 6(a). Isothermal holding at 80°C for about $6.6 \times 10^5$ s showed a weak but measurable flow of $^{222}$Rn atoms. Permeation of $^{222}$Rn essentially indicates that it is dissolving in the polycrystalline foil specimen. Although calculations by Rimmer and Cottrell [8] preclude any possibility of measurable solubility of radon in metals, grain boundary regions in polycrystals have a spectrum of atomic spacings [9] where much higher solubility may exist.

The variation of $W_I$ with $t$ measured with MCC2 during step-heating treatment $h_1$ [cf. Fig. 6(a)] is

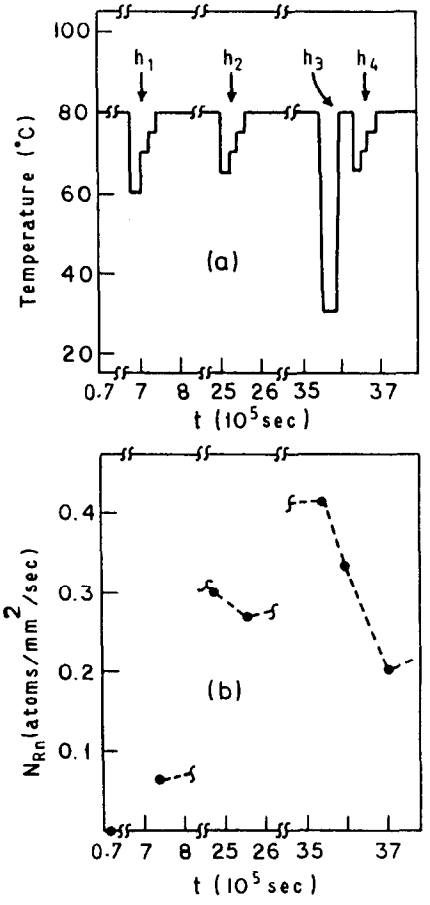


Fig. 6. (a) Thermal schedule of the foil specimen, (b) $N_{Rn}$ measured at 80°C at various instances of this schedule. The discontinuity in time-scale is apparent in the plot.

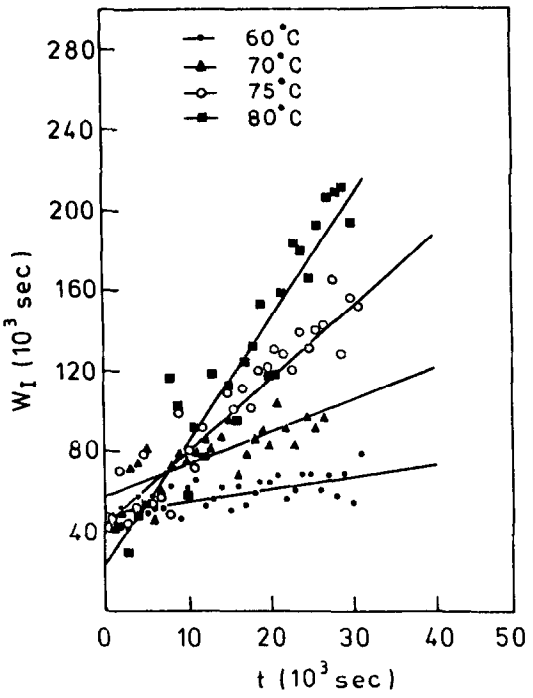


Fig. 7. $W_I$ vs $t$ recorded in the step-heating experiments $h_1$ of Fig. 6(a).

shown in Fig. 7. Here at each temperature MCC2 was cleared of residual $^{222}Rn$ atoms by flushing out with an $N_2$ jet. Figure 7 shows that the background in counting $W_I$ was low and unrelated to the magnitude of $W_I$. Scatter in the experimental data of the plot originates from the statistical nature of the nuclear decay of the small population of $^{222}Rn$ atoms in MCC. The number of $^{222}Rn$ atoms coming out per unit area of the foil per second $N_{Rn}$, has been calculated from $dW_I/dt(=I)$. The $N_{Rn}$s estimated from Fig. 7 are 6500, 17,000, 39,000 and 66,000 atoms $m^{-2}$ $s^{-1}$ at 60, 70, 75 and 80°C, respectively. These results demonstrate the sensitivity of this spectroscopic method.

The Arrhenius plot of $N_{Rn}$ for treatment $h_1$ yields an activation energy $Q_S = 115$ kJ $mol^{-1}$, which is higher than the grain-boundary self-diffusion energy in Au (84 kJ $mol^{-1}$) [10], but appreciably smaller than the lattice self-diffusion energy [11] in Au (176.6 kJ $mol^{-1}$), and it is of the order of the activation enthalpy for diffusion of Rn in cold-worked Ag (120 kJ $mol^{-1}$) [12]. The $Q_S$ obtained from the step-heating experiments [e.g. $h_1$, $h_2$ and $h_4$ in Fig. 6(a)] does not have a unique value nor does it represent the activation energy of $^{222}Rn$ permeation. The very small magnitude of flux observed may indicate that only some particular sites of the foil are involved in the diffusion.

Figure 6(b) shows $N_{Rn}$ measured at 80°C at various instances of the thermal schedule in Fig. 6(a). Apparently, the permeability in the foil depends on its thermal history and the changes seem to be reversible in nature. These results preclude the possibility of evaluating $C_0$, $C_1$ and $D$ through pulse-heating experiments like $h_3$ [Fig. 6(a)]. It is not yet understood whether the impurity segregation at grain boundaries or the trapping centres in the specimen causes the observed variation in permeability.

## 5. CONCLUSIONS

(1) The $\alpha$-spectroscopic method can readily measure $^{222}Rn$ permeation flux down to the order of $10^4$ atoms $m^{-2}$ $s^{-1}$.

(2) The time-lags of the constituent stages of the method are additive in nature.

(3) A $^{226}Ra$ needle can act as an infinite source for providing a nearly constant number of $^{222}Rn$ atoms in the source chamber (RSC) in the course of permeation measurements.

(4) The threshold electrode potential $B_m$ increases with the volume of the metallic collection chamber (MCC).

(5) The limiting value of net collection efficiency $f$ is enhanced with the decrease in the size of MCC and the increase in the active area of the $\alpha$-detector.

(6) The effective decay constant $k$ for a detector assembly deviates from the natural decay constant $\lambda_{Rn}$ primarily due to the leakage of $^{222}Rn$ atoms from the MCC rather than by adsorption or dissolution of $^{222}Rn$ at the MCC walls.

(7) $^{222}Rn$ has a detectable solubility in polycrystalline Au at low temperatures (e.g. 80°C).

(8) The permeability of $^{222}Rn$ in Au depends on the thermal history of the specimen.

*Acknowledgements*—The authors are indebted to Professor Dr H. Gleiter for the provision of laboratory facilities, for much invaluable advice and constant encouragement. Thanks are due to Dr K. Smidoda, Dr R. Dudler, Dr K. H. Folkerts and Dr G. Keller for many stimulating discussions. H. H. acknowledges the financial support from the Fritz-Thyssen Stiftung. S.K.P. is grateful to AvH-Stiftung for offering him a Humboldt Fellowship in support of this work. The financial support from the DFG, the BMFT and ALCOA Foundation is gratefully acknowledged.

## REFERENCES

1. Le Claire A. D., *Diffusion Defect Data* **33**, 1 (1983).
2. Crockett A. H., Smith K. C., Bartlett N. and Sladhy F. C., *Chemistry of the Monoatomic Gases*. Pergamon Press, New York (1975).
3. Seelmann-Eggebert W., Pfenning G. and Münzel H., *Karlsruher Nuklidkarte*. Kernforschung GmbH, Karlsruhe (1974).
4. Azenberg-Selove F., *Nuclear Spectroscopy, Part B*. Academic Press, New York (1960).
5. Keller G., Folkerts K. H. and Muth H., *Radiat. Protect. Dosimetry* **3**, 83 (1982).
6. Crank J., *Mathematics of Diffusion*, pp. 47 and 124. Oxford University Press, Oxford (1956).
7. Barrer R. M., *Trans. Faraday Soc.* **35**, 628 (1939).
8. Rimmer D. E. and Cottrell A. H., *Phil. Mag.* **2**, 1345 (1957).

9. Birringer R., Herr U. and Gleiter H., *Proc. JIMIS—4, Trans. Jpn. Inst. Met.* **27** (Suppl.), 43 (1986).
10. Martin G. and Perraillon B., *J. Phys. Colloq.* C4, **36,** 165 (1975).
11. Gilder H. M. and Lazarus D., *J. Phys. Chem. Solids* **26,** 2081 (1965).
12. Matzk Hj., Rickers G. and Sorensen G., *Acta Metall.* **20,** 1241 (1972).